ECS Transactions, 33 (6) 89-99 (2010)
10.1149/1.3487537 ©The Electrochemical Society

Growth of MnGe Nanostructures for Spintronics Applications

K. L. Wang and Faxian Xiu

Department of Electrical Engineering, University of California at Los Angeles, Los Angeles, CA, 90095-1594

Mainstream CMOS technology in today's electronics continues to scale down in the feature size. However, power dissipation per unit area and variability are among two major issues and challenges for the continuing scaling. Spintronics, as an emerging technology that exploits the intrinsic spin of the carriers, could potentially offer power savings, low variability and improved scalability. Using nanoscale materials makes possible heterogeneous integration of dissimilar materials by accommodation of strain and minimizing defects. In this paper, we present work on Mn_xGe_{1-x} nanostructures. We discuss our nanoscale deposition and nano-epi approach in preparing single-crystalline dilute magnetic $Mn_{0.05}Ge_{0.95}$ QDs. By the use of MOS capacitor with the $Mn_{0.05}Ge_{0.95}$ QDs as the channel material and by controlling the electrical field at the gate, we demonstrate the ferromagnetism of the QDs by modulating the hole concentration in the channel. A theoretical understanding of high-Curie temperature nature of $Mn_{0.05}Ge_{0.95}$ is also provided via DOS simulations.

Introduction

Recent challenges faced on scaling by the complementary metal–oxide–semiconductor (CMOS) technology have prompted the search for alternative solutions, one of which is the magneto-electronics (ME). The underlying idea is that the ME devices use the electron spin instead of the electron charge as a state variable and/or memory unit. It is understood that in order to be competitive with the CMOS, ME devices should be operable at room temperature (RT) and have the solid-state realization. The above requirements exclude the implementation of spins of single electrons, thus promoting the usage of the ferromagnetic order (FO) – the collective electron spins of ferromagnetic materials. The FO of tiny metallic parts has been employed for magnetic data storage purposes for decades 1 with the most recent achievement in this direction being the electric-current-controlled spin-transfer-torque (STT) memory [2-4]. The FO-based memory is advantageous [5] in the light of the (inhomogeneous) variability issues of electron-charge-based memory.

As opposed to the purposes of data storage, in which the high variability is the most outstanding problem at the nanometer scale, the information processing (or data manipulation) suffers mostly from the energy dissipation issue. The dissipation comes mainly from the electric currents controlling the operation of the device. From this perspective, the use of the FO in the combination with the electric-current control may deteriorate all the possible advantages of switching to the FO state variables. For example, STT cells, considered as state variables, will require too-high electric currents for their manipulation [6], which would make such manipulation of data even more power-consuming than the conventional processors. Furthermore, the characteristic energy of

the FO anisotropy is of orders of magnitude lower than that of the electron band structure. In result, it is very unlikely that the back-action of the FO can efficiently control the electric-charge-flow. This, in turn, makes unfeasible the "reverse" idea of using the FO for the control of the electron-current instead. The connotation of the above discussion is that it is likely necessary to master the control of the FO by the low-dissipative bias voltage in order to be able to make use of the FO as of a state variable for computations.

One of such possibilities is the multiferroic materials, which possess in addition the ferroelectric order coupled to the FO. The spatial orientation of the FO is thus controllable in multiferroics through the voltage control of the ferroelectric order [7-10]. Another idea being developed lately is the possibility of the voltage control of the very existence of the FO – the voltage-controlled ferromagnetic ordering (VCFO). One of the possible (and in a sense ultimate) devices enabled by the VCFO is what could be called an instanton-transistor. This device enables the gate-voltage control of the instanton-current flow (or the magnetization-orientation flow), that is of the non-local exchange coupling between the magnetization orientation of the "source" and "drain", as shown in Figure 1. The physical essence of the operation of the VCFO-material-based instanton-channel is that its Curie temperature (T_c) is close enough to the RT and the relative position of T_c and RT on the temperature scale can be reversibly interchanged by gate-voltage.

From material's realization point of view, on trying to locate the requirements, to which a VCFO material must satisfy, one expects that in reality the voltage variation of T_c is relatively small. This implies that the device operates in the critical region. In the critical region, the influence of the injected carriers on the magnetization is determined by the magnetic correlation length, $\xi \sim \Lambda(T_C / |T - T_C|)^{\nu}$, where ν is the critical exponent, which depends only the universality class of ferromagnetic transition, and Λ is the so-called cutoff - a characteristic length, which is approximately several lattice constants and which does vary considerably for different materials. The correlation length diverges near the transition point and can definitely be of order of dozens nanometers in the critical region. The above is true for all ferromagnets and consequently for the nanometer-scale realization of the VCFO all ferromagnets with T_c close to RT are more or less the same [11-15]. From another point of view, the coupling between the FO and the injected carriers must be strong. Again, all the itinerant-electron ferromagnets (even metals) satisfy this requirement. Supporting the above statements is the recent experimental demonstration of that in complex oxides, in which electron density is almost at the metallic level (10^{21} cm^{-3}), the T_c - variation is even higher than that in (Mn)GaAs DMS [16]. Nevertheless, due to their high compatibility of DMS with today's Si technology, it is likely that the reliable RT-VCFO will be first realized in the DMS materials.

Among the DMSs is the Mn doped Si and Ge, which have attracted extensive attention recently [17-27]. In these materials, both the T_c and the saturation magnetization depend on the interplay of a variety of factors, which are ultimately determined by the growth conditions and post-annealing process [28, 29]. The concentration and distribution of Mn dopants, the carrier density, the presence of common defects such as Mn interstitials and Mn clusters significantly influence the magnitude and interactions of the magnetic coupling [26, 30]. It is anticipated that this interplay between various growth parameters can be reduced in low dimensional structures [31]. In addition, nanostructures such as Mn doped Ge quantum dots (QDs) could offer unique and salient physical properties, arising from the size-related quantum confinement effects, and affect the carrier transport, spin-coherence lifetime, interactions between spins, and thus the ferromagnetic properties in general [32]. More importantly, the magnetic Mn_xGe_{1-x} can be directly incorporated with

the current CMOS platforms, promoting immediate applications in the microelectronics industry.

The first demonstration of the VCFO in that in (In, Mn)As materials, in which the T_c was varied by ±1 K with a voltage of ±125 V, corresponding to an electric field of approximately ±1.6 MV/cm [16]. The applicability of this phenomenon, however, is limited because of the low T_c of (In, Mn)As [33]. On the other hand, Mn-doped Ge DMS was reported to possess much higher T_c's. For example, in $Mn_{0.06}Ge_{0.94}$ single-crystalline thin films [34], T_c ~285 K. In other experimental studies, the magnetic properties of Mn_xGe_{1-x} nanostructures were carried out by the ion implantation of Mn [35]. The signature of the influence of the injected carriers on the ferromagnetic properties of Mn_xGe_{1-x} nanostructures was observed by applying gate biases in MOS capacitors at a low temperature of 10 K. However, the existence of the metallic precipitates such as Mn_5Ge_3 and $Mn_{11}Ge_8$ in these nanostructures, were expected to partly jeopardize the voltage-controlled hole-mediated exchange coupling. In this paper, we continue our previous work [35],[36], and demonstrate by the structural and magnetic characterizations the successful fabrication of the single-crystalline DMS QDs without signatures of the Mn_5Ge_3 or $Mn_{11}Ge_8$ precipitates. We investigate the T_c of the material by a superconducting quantum interference device (SQUID) magnetometer, and find that T_c, in principle, could be as high as 400 K. These high T_c's can be attributed to the quantum confinement of the carriers in the QD geometry, as confirmed by the numerical studies also presented in the paper. Further, we investigate the influence of the gate-bias on the ferromagnetic properties of the $Mn_{0.05}Ge_{0.95}$ DMS QDs up to 100 K. The measurements at higher temperatures (closer to the T_c) are not realized yet due to the leakage current limitations. Nevertheless, even away from the transition, we were able to see the influence of the gate-bias on the magnetic properties. The main aim of the present work is to provide a theoretical understanding of the high-Curie-temperature nature of these quantum dots, which also explains the gate modulated ferromagnetism.

Results and Discussion

Fabrication of $Mn_{0.05}Ge_{0.95}$ QDs

MnGe QDs were produced on *p*-type Si substrates by a solid-source MBE system. The Mn and Ge sources were provided by traditional effusion cells. The self-assembled MnGe QDs were grown at 450^{o}C with a Ge growth rate of 0.2 Å/s, similar to the growth of pure Ge QDs on Si under a typical Stranski-Krastanow (SK) mode. The MOS capacitors were fabricated by depositing 40 nm-thick Al_2O_3 on top of the $Mn_{0.05}Ge_{0.95}$ QD layer at 250 ^{o}C via an atomic layer deposition technique. The front and back sides were metalized with 200 nm-thick Au as the contact electrodes. The MOS capacitors were loaded into the SQUID magnetometer for bias-dependent magnetization measurements at different temperatures. We have noted that the quality of dielectric layer is very critical to minimize the leakage current. A thick Al_2O_3 of 40 nm ensures a relatively small leakage current below 10^{-6}A/cm^2.

Structural Properties of $Mn_{0.05}Ge_{0.95}$ QDs

Cross-section TEM was carried out to determine the structural characteristics and the Mn composition of the $Mn_{0.05}Ge_{0.95}$ QDs. It reveals a dome-shape dot on top of the Si substrate with a Mn diffusion area underneath as shown in Figure 1A. The dots have a typical base diameter of about 30 nm and a height of about 8 nm. Electron energy loss spectroscopy (EELS) shows that Mn dopants distribute uniformly inside the dots (Figure

1B). Selected area electron diffraction pattern (SAED) reveals a single-crystalline system (Figure 1C). The interface between the dot and the Si substrate shows excellent lattice coherence without pronounced dislocations or stacking faults (Figure 1E). Energy dispersive X-ray spectroscopy (EDS) confirms further the presence of Mn and Ge inside the dots. Based on an extensive composition analysis over many QDs, the percentage of Mn was determined to be about 5 % and no metallic phases, such as Mn_5Ge_3 and $Mn_{11}Ge_8$, were found. However, due to the extensive Mn doping, the formation of Mn clusters cannot be completely excluded which is beyond the detection limit of the conventional TEM.

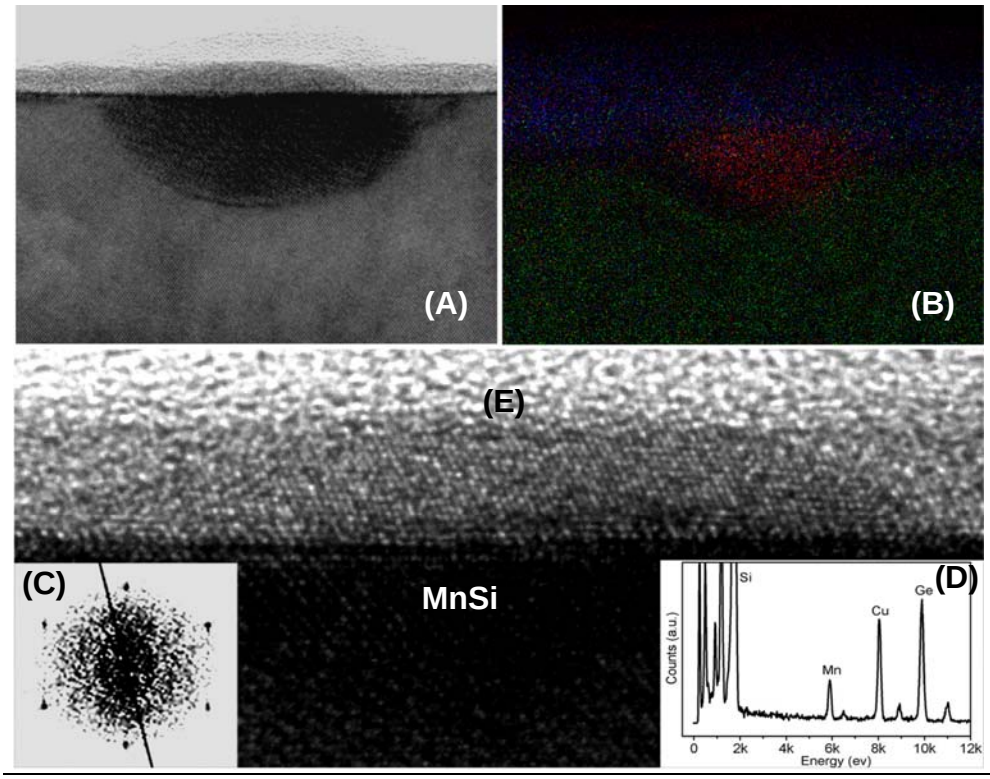

Figure 1. The structural properties of $Mn_{0.05}Ge_{0.95}$ QDs grown on a *p*-type Si substrate. (A) A high-resolution TEM (HR TEM) cross-section image of a $Mn_{0.05}Ge_{0.95}$ QD. Mn diffuses into the Si substrate, which is shown directly underneath the $Mn_{0.05}Ge_{0.95}$ QD. (B) The EELS composition mapping of Mn distribution. (C) The corresponding SAED pattern of $Mn_{0.05}Ge_{0.95}$ QD, revealing a single crystalline structure. (D) An EDS composition spectrum showing that both Mn and Ge are present in $Mn_{0.05}Ge_{0.95}$ QD. (E) An enlarged HR TEM image to show the detailed lattice structure of $Mn_{0.05}Ge_{0.95}$ QD.

Magnetic Properties of $Mn_{0.05}Ge_{0.95}$ QDs

Magnetic properties were carried out using a SQUID system. Figure 2A shows temperature-dependent hysteresis loops when the external magnetic field is parallel to the sample surface (in-plane). The field-dependent magnetization indicates a strong ferromagnetism above 400 K. The saturation magnetic moment per Mn atom is estimated to be 1.8 μ_B at 5 K. A fraction of roughly 60 % of Mn is estimated to be activated assuming that each Mn has a moment of 3 μ_B [18, 37-39]. Zero field cooled (ZFC) and field cooled (FC) magnetizations were measured with a magnetic field of 100 Oe as shown in Figure 2B. The magnetic moments do not drop to zero, suggesting a high T_c beyond 400

K. From these two curves, one can also infer the formation of a single phase in this material system, *i.e.*, DMS QDs, which is surprisingly similar to the high T_c DMS $Mn_{0.05}Ge_{0.95}$ nanowires [40]. The wide separation of the ZFC and FC curves in the temperature range of 5 to 400 K shows the irreversibility of susceptibilities, possibly arising from strain-induced anisotropy since a large lattice mismatch exists between Si and Ge [41].The temperature-dependent coercivity is shown in Figure 2B inset. Similar to the Mn_xGe_{1-x} nanowires [42], the coercivity decreases from 170 Oe (at 5 K) to 73 Oe (at 400 K). The small coercivity in the entire temperature range measured features a soft ferromagnetism which originates from Mn ions diluted in the Ge matrix [43]. The above magnetic properties support the fact that the $Mn_{0.05}Ge_{0.95}$ QDs exhibit a DMS type ferromagnetic order.

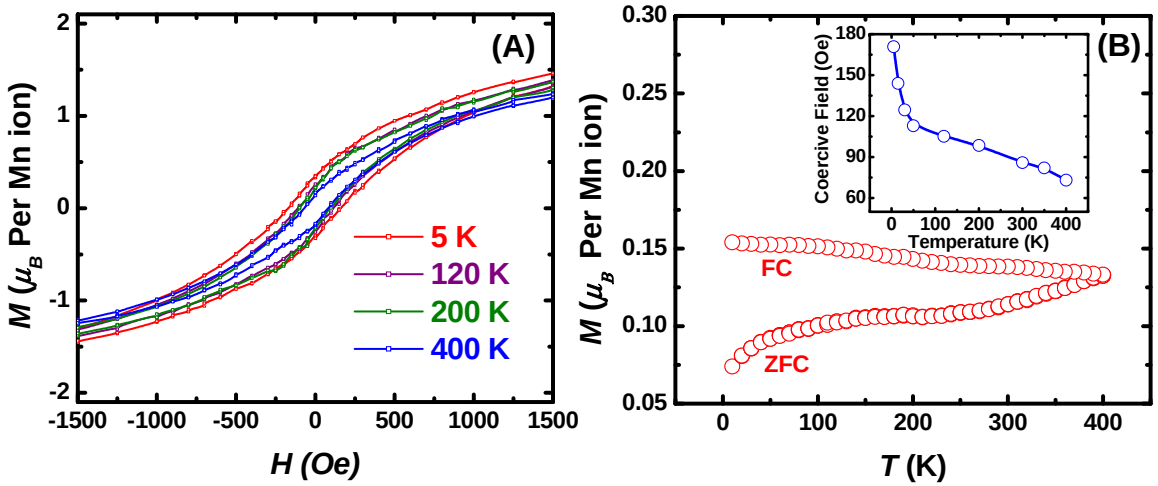

Figure 2. Magnetic properties of the $Mn_{0.05}Ge_{0.95}$ QDs grown on a p-type Si substrate. (A) Hysteresis loops measured at different temperatures from 5 to 400 K. The observation of a hysteresis loop at 400 K indicates a strong ferromagnetism above room temperature. (B) Zero-field cooled and field cooled magnetizations of QDs with a magnetic field of 100 Oe; the inset shows the coercivity values at different temperatures.

Atomic force microscopy (AFM) and magnetic force microscopy (MFM) measurements were carried out to investigate the morphology and ferromagnetism of the $Mn_{0.05}Ge_{0.95}$ QDs at 320 K, respectively. The average dot size is about 50 nm in base diameter and 6 nm in height. The dot density is about 6×10^9 cm^{-2} (Figure 3A). The corresponding MFM image was taken by lifting up the MFM probe 25 nm above the topographic height of the sample in a phase detection mode (Figure 3B). The appearance of bright-and-dark areas in the MFM image clearly shows the formation of magnetic domains in the $Mn_{0.05}Ge_{0.95}$ QDs, which is similar to (In, Mn)As DMS QDs [44]. Since the experiments were performed at 320 K, the formation of metallic phases such as Mn_5Ge_3 and $Mn_{11}Ge_8$ can be easily ruled out because they have low T_c of 296~300 K [29]. Overall, the above MFM results agree well with the TEM observations and the ferromagnetic order at high temperature obtained in the SQUID measurements.

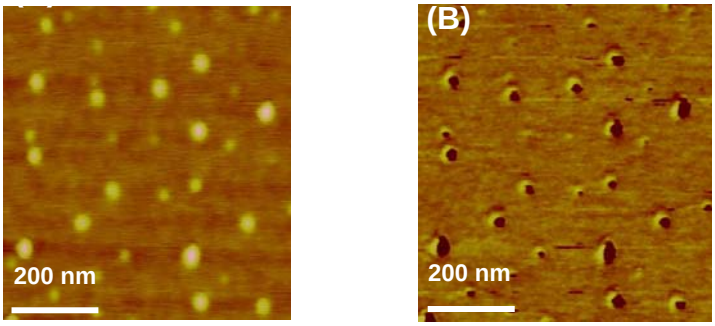

Figure 3. AFM and MFM images of the $Mn_{0.05}Ge_{0.95}$ QDs measured at 320 K. (A) Typical AFM image of $Mn_{0.05}Ge_{0.95}$ QDs. (B) Corresponding MFM image. Mn_5Ge_3 and $Mn_{11}Ge_8$ can be excluded because of their low Curie temperatures of 296~300 K.

Voltage-Controlled Ferromagnetic Ordering

Figures 4A and 4B show the hysteresis loops by SQUID with negative and positive biases on the MOS gate at 50 K, respectively. Under a negative bias, the holes are attracted into the channel of the device (accumulation). In this circumstance, however, the hysteresis loop does not show a remarkable change (Figure 4A). This could be explained by the fact that even at 0 V, the QDs device is already accumulated with enough holes to induce ferromagnetism. In other words, the hole-mediated effect is sufficient to align a majority of the activated Mn ions along one direction in each individual QD. Further increasing negative bias does not change much the hole concentrations.

On the contrary, with the positive bias, a large amount of holes are depleted into the *p*-type Si so that hole mediated effect is notably reduced. As a result, the Mn ions start to misalign because of the lack of holes. The saturation moment per Mn ion decreases more than 10 times as the gate bias increases from 0 to + 40 V (Figure 4B). It should be noted that, at + 40 V, the saturation and remnant moments of the $Mn_{0.05}Ge_{0.95}$ QDs become fairly weak, resembling a “paramagnetic-like” state. Figure 4C summarizes the change of remnant moments as a function of gate voltage. The inset in Figure 4C displays an enlarged picture to clearly show the change of remnant moments with respect to the gate bias. The above results evidently demonstrate that the hole mediated effect does exist in this material system, which is also supported from our previous experiments [35].

The desired high concentration of electrons on the surface, needed to deplete the DMS, is limited in our case solely by the leakage current. This is, in fact, the reason why we studied the voltage-effect well below the ferromagnetic transition, which is expected to be somewhere around ~400K, as implied by our SQIUD measurements (see previous section). By increasing the measurement temperature to 100 K (not shown here), the modulation of the ferromagnetism turned our to be less pronounced as compared to that at 50 K, which we believe is due to the increased leakage current in our MOS devices.

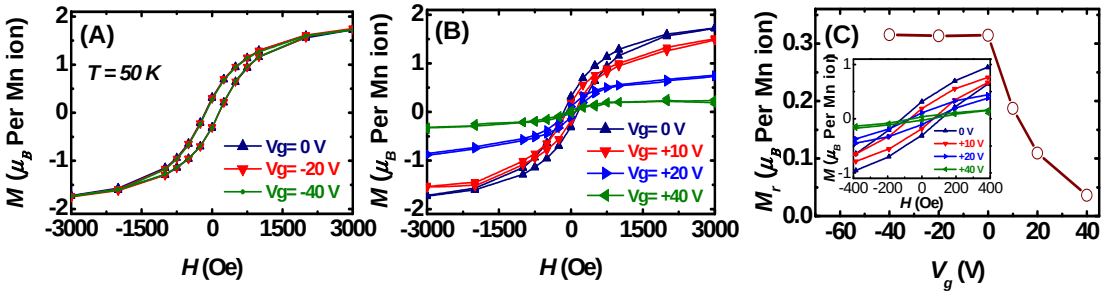

Figure 4. The manipulation of ferromagnetism of MnGe QDs by applying electrical fields. (A) Hysteresis loops with zero and negative bias of -20 and -40 V on the gate. (B) The hysteresis loops with zero and positive bias of +10, +20, and +40 V. (C) A representation of remnant moments with respect to the gate bias. Inset is the enlarged figure for the central part of (B) to clearly show the change of remnant moment. It is found that the remnant moments can be manipulated by applying bias on the MOS gate. The saturation moments can be also manipulated by the gate bias.

Role of the Quantum Confinement: Numerical Results

The fact that Curie temperatures in nanostructures [42, 44, 45] are typically higher than in the bulk materials can be attributed to the effects of quantum confinement [46]. To demonstrate this in our case of MnGe QDs, we performed first-principle calculations comparing the electronic structure of the bulk $Mn_{0.06}Ge_{0.94}$ and small MnGe QDs (diameter ~9 Å).

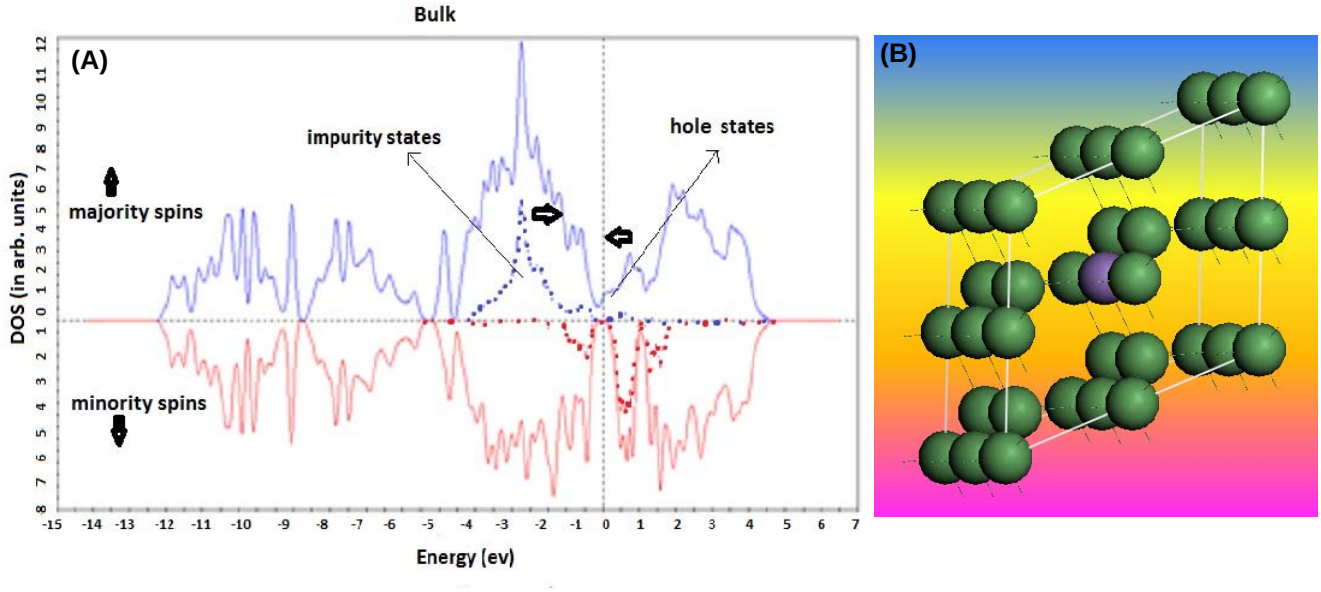

Figure 5. (A), Given is the total density of states (solid curve) and the DOS of the impurity levels (dashed curve) in bulk $Mn_{0.06}Ge_{0.94}$ as found using the CASTEP [47]. As one goes to nanometer sizes, the density of state of the localized *d*-like impurities and the itinerant *p*-like carriers are expected (see next Figure) to move toward each other on the energy scale, as indicated by the black arrows. (B), Simulated supercell structure.

The bulk $Mn_{0.06}Ge_{0.94}$ system was simulated within local spin-density approximation (LSDA) to density functional theory using periodic boundary condition. The kinetic energy cutoff used for the wavefunctions was 280 eV. The simulated supercell contained 16 atoms at the experimental Ge lattice constant (a=5.6 Å) with the central atom replaced

by Mn (corresponding to the case of a substitutional impurity, see Figure 5(B)). The other extreme of $Mn_1Ge_{28}H_{36}$ (diameter ~9 Å) QD was also simulated within LSDA to density functional theory using confined boundary condition (*i.e.* real-space wave functions going to zero outside a sphere enclosing the quantum dot). The structure of the QD was constructed by taking spherical fragment of the corresponding bulk diamond structure of Ge with surface passivated by hydrogen atoms and central atom replaced by Mn (Figure 6(B)). The surface was passivated to get rid of the surface states (introduced by dangling bonds at the surface) in the band gap [46]. The radius of the sphere enclosing this dot (outside which wavefunctions go to zero) and the grid spacing were varied until the corresponding eigenvalues converged. These values were 10 Å and 0.15 Å for the radius of enclosing sphere and grid spacing respectively.

The calculated total and *d*-like impurity density of states (DOS) for bulk shows *d*-like impurity states lying well below the Fermi-level (indicated by dashed vertical line in Figure 5(A)). This location of impurity states in turn implies that the carriers (holes at the Fermi-level) have more *p*-like character of the host Ge because of less mixing (hybridization) with the *d*-like Mn impurity states. The expected effect of quantum confinement on the DOS is to move these impurity states towards the Fermi-level (as indicated by arrows in Figure 5(A)) [46], [48] and hence increase the hybridization between the carriers (holes at the Fermi-level) and impurity states. This increase in hybridization between carriers and impurity states would in turn lead to increase in Curie temperature, T_c within the free-carrier mediated picture of the FO initially [46]. On the other hand T_c cannot increase monotonically with decreasing size as the increase in hybridization should also reduce the moving ability of the carriers making them more localized, thus, in turn, leading to the reduction of the effective exchange coupling between the neighboring magnetic dopants. Our numerical results for the limit of very small QD (diameter ~9 Å) confirm this increase in hybridization and corresponding increase in localization of the carriers. Figure 6(A) shows that the holes and the impurity states both overlap and are detached from the Ge valence bands lying at the Fermi level, thus assuming strong hybridization and the absence of hole mobility. This is further confirmed by the analysis of the spatial form of the hole wavefunctions near the Fermi level (Figure 6(A)).The above picture implies that there must be a region of intermediate sizes (and possibly shapes), where the *Tc* should peak.

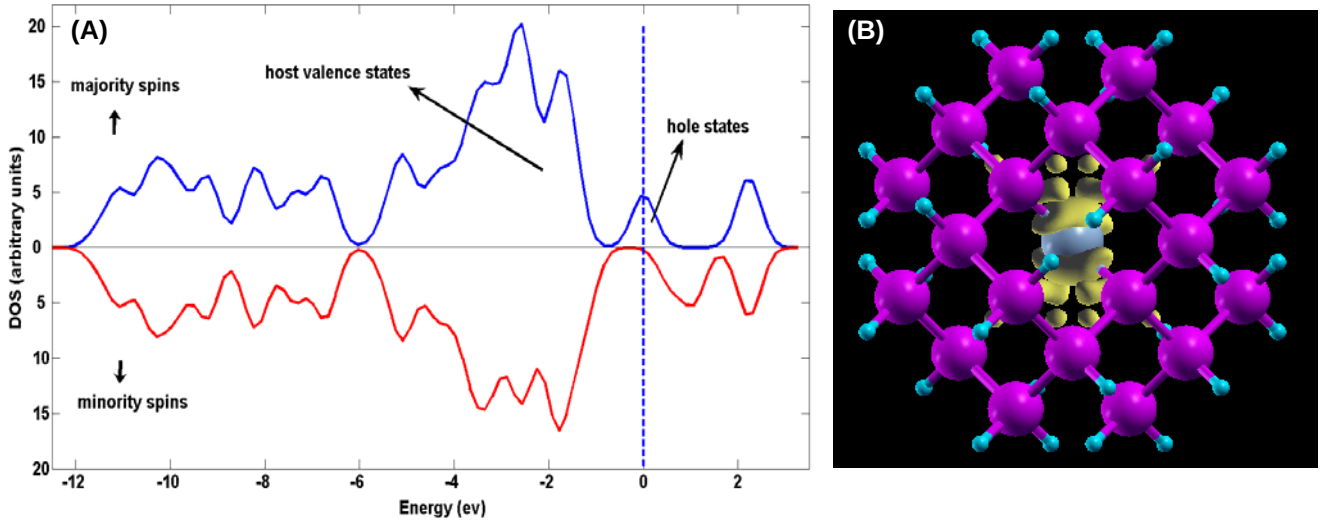

Figure 6. The demonstration of the effect of quantum confinement on the carrier localization (using PARSEC [49]). (A), DOS of $Ge_{28}Mn_1H_{36}$ (diameter ~9 Å), the p-like holes are trapped on the impurity d-like states and are detached from host valence band. (B), Yellow surface represents the typical iso-surface of hole wavefunction squared showing the localized character of holes around the only impurity in the cluster (central blue atom).

Conclusions

In summary, we discussed the technological importance of the possibility to control ferromagnetic state by low-dissipation bias voltages, and the important role of the dilute magnetic semiconductors as the most likely candidates for the realization of this phenomenon. We presented our recent experimental achievements on the voltage control of the ferromagnetic properties of single-crystalline $Mn_{0.05}Ge_{0.95}$ self-assembled QDs, grown on Si substrate by the MBE. Using superconducting quantum interference device magnetometer we found that T_c can in principle be as high as 400 K. We were able to investigate the influence of the gate-bias on the ferromagnetic properties of the $Mn_{0.05}Ge_{0.95}$ DMS QDs at temperatures up to 100 K – the limitation imposed by the thermo-activated leakage current. In combination with the numerical studies of DOS in this DMS, our experiments suggest that the efficient voltage controlled ferromagnetic ordering at room temperature can be realized in this material.

Acknowledgments

We gratefully acknowledge the financial support from the Western Institute of Nanoelectronics (WIN) and the Intel Spin-Gain FET project. We also thank our Australian collaborators Prof. Jin Zou and Dr. Yong Wang for their significant contributions of TEM experiments.

References

1. C. Chappert, A. Fert and F. N. Van Dau, Nat Mater **6** (11), 813-823 (2007).
2. I. N. Krivorotov, N. C. Emley, J. C. Sankey, S. I. Kiselev, D. C. Ralph and R. A. Buhrman, Science **307** (5707), 228-231 (2005).
3. I. N. Krivorotov, N. C. Emley, A. G. F. Garcia, J. C. Sankey, S. I. Kiselev, D. C. Ralph and R. A. Buhrman, Physical Review Letters **93** (16), - (2004).
4. S. I. Kiselev, J. C. Sankey, I. N. Krivorotov, N. C. Emley, M. Rinkoski, C. Perez, R. A. Buhrman and D. C. Ralph, Physical Review Letters **93** (3), - (2004).
5. I. V. Ovchinnikov and K. L. Wang, Applied Physics Letters **92** (9), - (2008).
6. F. J. Albert, J. A. Katine, R. A. Buhrman and D. C. Ralph, Applied Physics Letters **77** (23), 3809-3811 (2000).
7. J. Seidel, L. W. Martin, Q. He, Q. Zhan, Y. H. Chu, A. Rother, M. E. Hawkridge, P. Maksymovych, P. Yu, M. Gajek, N. Balke, S. V. Kalinin, S. Gemming, F. Wang, G. Catalan, J. F. Scott, N. A. Spaldin, J. Orenstein and R. Ramesh, Nature Materials **8** (3), 229-234 (2009).
8. L. Martin, S. P. Crane, Y. H. Chu, M. B. Holcomb, M. Gajek, M. Huijben, C. H. Yang, N. Balke and R. Ramesh, Journal of Physics-Condensed Matter **20** (43), - (2008).

9. Y. H. Chu, L. W. Martin, M. B. Holcomb, M. Gajek, S. J. Han, Q. He, N. Balke, C. H. Yang, D. Lee, W. Hu, Q. Zhan, P. L. Yang, A. Fraile-Rodriguez, A. Scholl, S. X. Wang and R. Ramesh, Nature Materials **7** (8), 678-678 (2008).
10. Y. H. Chu, Q. Zhan, L. W. Martin, M. P. Cruz, P. L. Yang, G. W. Pabst, F. Zavaliche, S. Y. Yang, J. X. Zhang, L. Q. Chen, D. G. Schlom, I. N. Lin, T. B. Wu and R. Ramesh, Advanced Materials **18** (17), 2307-+ (2006).
11. I. V. Ovchinnikov and K. L. Wang, Physical Review B (Condensed Matter and Materials Physics) **78** (1), 012405 (2008).
12. I. V. Ovchinnikov and K. L. Wang, Physical Review B (Condensed Matter and Materials Physics) **80** (1), 012405 (2009).
13. I. V. Ovchinnikov and K. L. Wang, Physical Review B **79** (2), - (2009).
14. Y. Sun, J. D. Burton and E. Y. Tsymbal, Physical Review B **81** (6), - (2010).
15. J. D. Burton and E. Y. Tsymbal, Physical Review B **80** (17), - (2009).
16. H. Ohno, D. Chiba, F. Matsukura, T. Omiya, E. Abe, T. Dietl, Y. Ohno and K. Ohtani, Nature **408** (6815), 944-946 (2000).
17. M. Bolduc, C. Awo-Affouda, A. Stollenwerk, M. B. Huang, F. G. Ramos, G. Agnello and V. P. LaBella, Phys. Rev. B **71** (3), 033302 (2005).
18. Y. D. Park, A. T. Hanbicki, S. C. Erwin, C. S. Hellberg, J. M. Sullivan, J. E. Mattson, T. F. Ambrose, A. Wilson, G. Spanos and B. T. Jonker, Science **295** (5555), 651-654 (2002).
19. J. S. Kang, G. Kim, S. C. Wi, S. S. Lee, S. Choi, S. Cho, S. W. Han, K. H. Kim, H. J. Song, H. J. Shin, A. Sekiyama, S. Kasai, S. Suga and B. I. Min, Physical Review Letters **94** (14), 147202 (2005).
20. M. Passacantando, L. Ottaviano, F. D'Orazio, F. Lucari, M. D. Biase, G. Impellizzeri and F. Priolo, Physical Review B (Condensed Matter and Materials Physics) **73** (19), 195207 (2006).
21. N. Pinto, L. Morresi, M. Ficcadenti, R. Murri, F. D.Orazio, F. Lucari, L. Boarino and G. Amato, Phys. Rev. B **72** (16), 165203 (2005).
22. Y. Wang, J. Zou, Z. Zhao, X. Han, X. Zhou and K. L. Wang, Journal of Applied Physics **103** (6), 066104 (2008).
23. C. Zeng, W. Zhu, S. C. Erwin, Z. Zhang and H. H. Weitering, Phys. Rev. B **70** (20), 205340 (2004).
24. A. P. Li, J. F. Wendelken, J. Shen, L. C. Feldman, J. R. Thompson and H. H. Weitering, Phys. Rev. B **72** (19), 195205 (2005).
25. S. Ahlers, D. Bougeard, N. Sircar, G. Abstreiter, A. Trampert, M. Opel and R. Gross, Physical Review B (Condensed Matter and Materials Physics) **74** (21), 214411 (2006).
26. C. Bihler, C. Jaeger, T. Vallaitis, M. Gjukic, M. S. Brandt, E. Pippel, J. Woltersdorf and U. Gosele, Applied Physics Letters **88** (11), 112506 (2006).
27. P. De Padova, J. P. Ayoub, I. Berbezier, P. Perfetti, C. Quaresima, A. M. Testa, D. Fiorani, B. Olivieri, J. M. Mariot, A. Taleb-Ibrahimi, M. C. Richter, O. Heckmann and K. Hricovini, Phys. Rev. B **77** (4), 045203 (2008).
28. M. Bolduc, C. Awo-Affouda, F. Ramos and V. P. LaBella, 2006 (unpublished).
29. M. Jamet, A. Barski, T. Devillers, V. Poydenot, R. Dujardin, P. Bayle-Guillemaud, J. Rothman, E. Bellet-Amalric, A. Marty, J. Cibert, R. Mattana and S. Tatarenko, Nat Mater **5** (8), 653-659 (2006).
30. E. Biegger, L. Staheli, M. Fonin, U. Rudiger and Y. S. Dedkov, Journal of Applied Physics **101** (10), 103912 (2007).
31. K. Brunner, Reports on Progress in Physics **65** (1), 27-72 (2002).

32. R. Knobel, N. Samarth, S. A. Crooker and D. D. Awschalom, Physica E: Low-dimensional Systems and Nanostructures **6** (1-4), 786-789 (2000).
33. M. Weisheit, S. Fahler, A. Marty, Y. Souche, C. Poinsignon and D. Givord, Science **315** (5810), 349-351 (2007).
34. S. Cho, S. Choi, S. C. Hong, Y. Kim, J. B. Ketterson, B.-J. Kim, Y. C. Kim and J.-H. Jung, Phys. Rev. B **66** (3), 033303 (2002).
35. J. Chen, K. L. Wang and K. Galatsis, Applied Physics Letters **90** (1), 012501 (2007).
36. F. Xiu, Y. Wang, J. Kim, A. Hong, J. Tang, A. P. Jacob, J. Zou and K. L. Wang, Nat Mater **9** (4), 337-344.
37. A. Stroppa, S. Picozzi, A. Continenza and A. J. Freeman, Phys. Rev. B **68** (15), 155203 (2003).
38. T. C. Schulthess and W. H. Butler, Jounal of Applied Physics **89**, 7021-7023 (2001).
39. M. v. Schilfgaarde and O. N. Mryasov, Phys. Rev. B **63** (23), 233205 (2001).
40. Y. J. Cho, C. H. Kim, H. S. Kim, W. S. Lee, S.-H. Park, J. Park, S. Y. Bae, B. Kim, H. Lee and J.-Y. Kim, Chemistry of Materials **20** (14), 4694-4702 (2008).
41. T. Dietl, H. Ohno and F. Matsukura, Phys. Rev. B **63** (19), 195205 (2001).
42. M. I. van der Meulen, N. Petkov, M. A. Morris, O. Kazakova, X. Han, K. L. Wang, A. P. Jacob and J. D. Holmes, Nano Letters **9** (1), 50-56 (2008).
43. O. Kazakova, J. S. Kulkarni, J. D. Holmes and S. O. Demokritov, Phys. Rev. B **72** (9), 094415 (2005).
44. H. C. Jeon, Y. S. Jeong, T. W. Kang, T. W. Kim, K. J. Chung, W. Jhe and S. A. Song, Advanced Materials **14** (23), 1725-1728 (2002).
45. Y. H. Zheng, J. H. Zhao, J. F. Bi, W. Z. Wang, Y. Ji, X. G. Wu and J. B. Xia, Chinese Physics Letters **24** (7), 2118-2121 (2007).
46. S. Sapra, D. D. Sarma, S. Sanvito and N. A. Hill, Nano Letters **2** (6), 605-608 (2002).
47. P. J. P. L. M D Segall, M J Robert ,C J Pickard, D J Hasnip, S J Clark, M C Payne, Journal of Physics: Condensed Matter **14**, 2717 (2002).
48. X. Huang, A. Makmal, J. R. Chelikowsky and L. Kronik, Physical Review Letters **94** (23), 236801 (2005).
49. J. R. Chelikowsky, N. Troullier and Y. Saad, Physical Review Letters **72** (8), 1240 (1994).